References and Notes

1. C. H. June *et al*., *Proc. Natl. Acad. Sci. U.S.A.* **87**, 7722 (1990); D. B. Straus and A. Weiss, *Cell* **70**, 585 (1992); K. Chu and D. R. Littman, *J. Biol. Chem.* **269**, 24095 (1994).
2. C. T. Baldari *et al*., *Oncogene* **10**, 1141 (1995).
3. J. Jackman *et al*., *J. Biol. Chem.* **270**, 7029 (1995).
4. J. A. Donovan, R. L. Wange, W. Y. Langdon, L. E. Samelson, *ibid*. **269**, 22921 (1994).
5. M. Musci *et al*., *ibid*. **272**, 11674 (1997).
6. W. Zhang, J. Sloan-Lancaster, J. Kitchen, R. P. Trible, L. E. Samelson, *Cell* **92**, 83 (1998).
7. J. Wu, D. G. Motto, G. A. Koretzky, A. Weiss, *Immunity* **4**, 593 (1996); H. Onodera, D. G. Motto, G. A. Koretzky, D. M. Rothstein, *J. Biol. Chem.* **271**, 22225 (1996); L. Tuosto, F. Michel, O. Acuto, *J. Exp. Med.* **184**, 1161 (1996).
8. D. G. Motto, S. E. Ross, J. Wu, L. R. Hendricks-Taylor, G. A. Koretzky, *J. Exp. Med.* **183**, 1937 (1996).
9. A. J. da Silva *et al*., *Proc. Natl. Acad. Sci. U.S.A.* **94**, 7493 (1997).
10. M. A. Musci, D. G. Motto, S. E. Ross, N. Fang, G. A. Koretzky, *J. Immunol.* **159**, 1639 (1997).
11. J. L. Clements, S. E. Ross-Barta, G. A. Koretzky, in preparation. We have also detected SLP-76 expression in the NK cell lineage in normal mice. However, the intensity of SLP-76 staining observed in NK cells is ~50% of that observed in resting T cells.
12. A pair of polymerase chain reaction (PCR) primers (forward, 5′-TCGACTCGATCAGACCTGAAGATGAAG-3′; reverse 5′-GCTTCTGTCTATTGATGGAGCAGG-3′) were designed to amplify a 320-bp product composed of SLP-76 genomic sequence including an exon encoding amino acids 208 to 229, the following 96-bp intron, and a portion of the next exon encoding amino acids 230 to 257. These primers were used to obtain a commercial P1 murine SLP-76 genomic library (strain 129/SVJ, Genome Systems, St. Louis). To generate a targeting vector specific for the SLP-76 genomic locus, we amplified from the P1 clone a 1.6-kb PCR fragment comprising sequence immediately upstream of the SLP-76 translational start site and subcloned it into the Bam HI and Eco RI restriction sites in the pPNT parental vector. Next, a 3-kb Xho I–flanked, PCR-amplified product composed of SLP-76 intronic sequence located between exon 1 and exon 2 was subcloned into the Xho I site of pPNT. The targeting construct was then transfected by electroporation into ES cells. G418- and gancyclovir-resistant colonies were isolated and screened by Southern (DNA) blot analysis for a correctly targeted SLP-76 allele. Targeted clones were microinjected into blastocyts obtained from C57/BL6 mice, which were then transferred to pseudopregnant CD-1 recipient mice. Chimeric offspring were mated with wild-type C57/B6 mice, and heterozygous offspring were identified by Southern blot analysis of tail genomic DNA.
13. Total RNA was prepared from freshly isolated thymocytes, splenocytes, or the indicated cell line with Stat-60 (Tel-Test) according to the manufacturer's protocol. Approximately 2 μg of total RNA was used for cDNA synthesis in a 20-μl reaction mixture containing 50 ng of oligo(dT) primers (Life Technologies) and 200 U of Moloney murine leukemia virus reverse transcriptase (Life Technologies). A 5-μl sample of the cDNA synthesis reaction was then used for PCR with primers specific for 5′ SLP-76 sequence (forward, 5′-TTTCGCTCAGAGGTCCTAGCC-3′; reverse, 5′-GCTTCTGTCTATTGATGGAGCAGG-3′), 3′ SLP-76 sequence (forward, 5′-TCGGATCCCAGGGCCTCTCAAGGCCTCCTC-3′; reverse, 5′-GTCGGATCCTAAGTGCTCGGCGATTTG-3′), preTα (forward, 5′-GCTGCTTCTGGGCGTCAGG-3′; reverse, 5′-CAGGCCTGGTGTGACAGACC-3′), or Grb2 as a control (forward, 5′-GGCGGATCCGAAGCCATCGCCAAATATGACTTC-3′; reverse, 5′-GGGAATTCAGACGTTCCGGTTCACGGGGGTGAC-3′).
14. J. L. Clements *et al*., data not shown.
15. The following antibodies were used for FACS analysis: Rat antibodies to mouse CD11b (Mac-1, M1/70.15.11.5.HL), CD4 (GK1.5), CD8 (53.6.72), CD44 (9F3), B220 (6B2), and CD25 (7D4) were partially purified from serum-free supernatants (HB101) and were conjugated where indicated with fluorescein isothiocyanate (FITC), biotin, Cyanine 5-18, or phycoerythrin (PE) using standard procedures. The FITC-conjugated rat antibody to mouse pan (anti–mouse pan) specific for NK cells (DX-5), FITC-conjugated hamster anti–mouse CD3ε (145-2C11), PE-conjugated rat anti–mouse Thy-1.2 (53-2.1), and biotin-conjugated hamster anti–mouse TCRβ (H57-597) were purchased from Pharmingen. All samples were analyzed with a Coulter EPICS 753 instrument, and FACS data were analyzed with Flojo version 2.3.3 software (Treestar).
16. H. J. Fehling, A. Krotkova, C. Saint-Ruf, H. von Boehmer, *Nature* **375**, 795 (1995).
17. E. S. Hoffman *et al*., *Genes Dev.* **10**, 948 (1996).
18. P. Mombaerts *et al*., *Cell* **68**, 869 (1992); Y. Shinkai *et al*., *ibid*., p. 855 (1992); T. Molina *et al*., *Nature* **357**, 161 (1992).
19. Genomic DNA was prepared from SLP-76 +/− or −/− thymocytes and the ES cell line 129. We performed PCR using primers and conditions previously described (*27*) in a total volume of 50 μl. Next, 15 μl of the reaction products was resolved by electrophoresis in a 1.5% agarose gel, transferred to a nylon membrane, and probed with a radiolabeled oligomer corresponding to the $J_\beta 2.6$ gene segment (5′-GAACAGTACTTCGGTCCCGGCACCAGGCTC-3′) in a 6× standard saline citrate (SSC)–based hybridization buffer.
20. For proliferation assays, 0.2×10^6 splenocytes from SLP-76 +/− or −/− mice were incubated in 200 μl of RPMI supplemented with 10% fetal bovine serum and 2-ME or stimulated with lipopolysaccharide (10 μg/ml), anti-CD40 (Pharmingen, 1 μg/ml), or plate-bound anti-CD3ε [145-2C11, plated in phosphate-buffered saline (PBS) at 8 μg/ml]. After 48 or 72 hours of culture, cells were pulsed with 1 μCi of [^{3}H]thymidine (Amersham) and incubated for an additional 4 hours before they were harvested and analyzed by liquid scintillation. To quantitate concentrations of circulating immunoglobulin M (IgM), we serially diluted sera obtained from SLP-76 +/+, +/−, and −/− mice and incubated the sera in the presence of a plate-bound, isotype-specific capture antibody (μ-chain specific, Jackson Laboratories). Plates were washed and incubated with an alkaline phosphatase–conjugated antibody specific for mouse Ig (Pharmingen). After extensive washing, bound antibody was detected with p-PNP substrate (Pharmingen), and absorbance was determined at 405 nm. The IgM concentrations were determined by comparison with an IgM standard curve.
21. C. Saint-Ruf *et al*., *Science* **266**, 1208 (1994).
22. N. S. van Oers, H. von Boehmer, A. Weiss, *J. Exp. Med.* **182**, 1585 (1995).
23. M. Raab, A. J. da Silva, P. R. Findell, C. E. Rudd, *Immunity* **6**, 155 (1997).
24. I. Negishi *et al*., *Nature* **376**, 435 (1995).
25. A. M. Cheng *et al*., *Proc. Natl. Acad. Sci. U.S.A.* **94**, 9797 (1997).
26. N. S. van Oers, B. Lowin-Kropf, D. Finlay, K. Connolly, A. Weiss, *Immunity* **5**, 429 (1996).
27. S. J. Anderson, S. D. Levin, R. M. Perlmutter, *Nature* **365**, 552 (1993).

28. We thank K. Latinis, E. Peterson, and M. Welsh for critical reading of the manuscript; T. Waldschmidt for antibodies; R. Mulligan for the pPNT plasmid; A. Nagy for the ES cell line; and D. Yablonski and A. Weiss for communicating results before publication. We also thank P. Ruther for technical assistance and animal care and J. Fishbaugh and G. Hess for assistance with flow cytometry. Supported in part by NIH grants GM53256 (G.A.K.) and HL09431 (B.Y.), the Arthritis Foundation (J.L.C.), and the American Heart Association (G.A.K.).

8 April 1998; accepted 29 May 1998

Corelease of Two Fast Neurotransmitters at a Central Synapse

Peter Jonas,* Josef Bischofberger, Jürgen Sandkühler†

It is widely accepted that individual neurons in the central nervous system release only a single fast transmitter. The possibility of corelease of fast neurotransmitters was examined by making paired recordings from synaptically connected neurons in spinal cord slices. Unitary inhibitory postsynaptic currents generated at interneuron-motoneuron synapses consisted of a strychnine-sensitive, glycine receptor–mediated component and a bicuculline-sensitive, γ-aminobutyric acid $(GABA)_A$ receptor–mediated component. These results indicate that spinal interneurons release both glycine and GABA to activate functionally distinct receptors in their postsynaptic target cells. A subset of miniature synaptic currents also showed both components, consistent with corelease from individual synaptic vesicles.

Synaptic transmission in the central nervous system (CNS) is mediated by the release of neurotransmitters into the synaptic cleft and the subsequent activation of postsynaptic receptors. A single neurotransmitter can coactivate multiple ionotropic and metabotropic receptor types (*1*), and a fast neurotransmitter can be coreleased with neuropeptides (*2*). In the spinal cord and brainstem, both glycine and GABA mediate inhibitory synaptic transmission (*3*). It is not known, however, whether glycine and GABA are released from separate or overlapping populations of interneurons. Glycine- and GABA-like immunoreactivity coexist in the somata and boutons of subpopulations of spinal interneurons, and glycine receptor (GlyR) subunit, $GABA_A$ re-

Physiologisches Institut der Universität Freiburg, D-79104 Freiburg, Germany.

*To whom correspondence should be addressed. E-mail: jonasp@ruf.uni-freiburg.de

†On sabbatical leave from II. Physiologisches Institut, D-69120 Heidelberg, Germany.

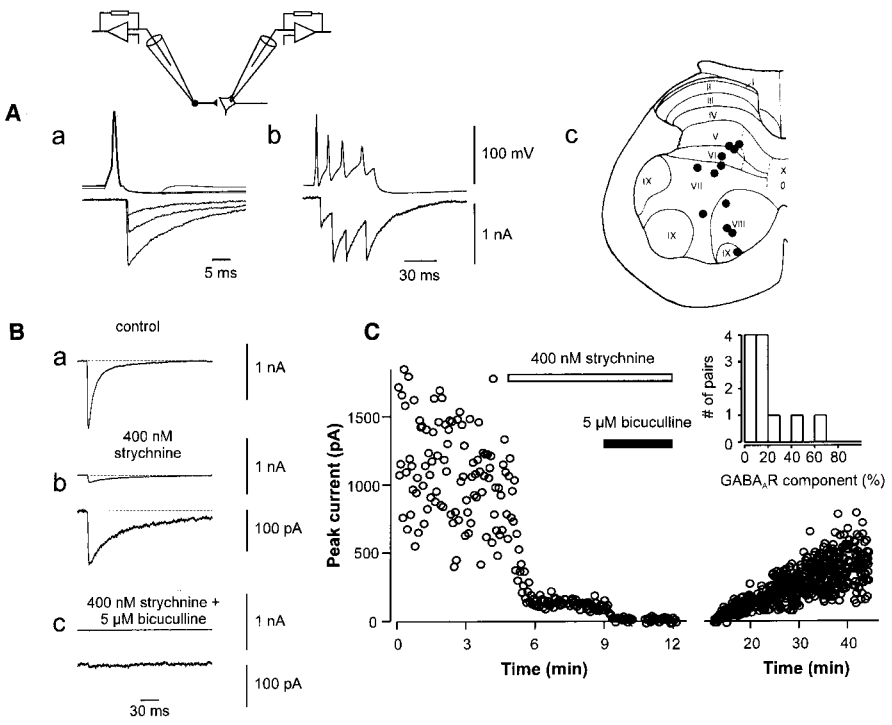

Fig. 1. GlyR- and $GABA_A$R-mediated components of unitary IPSCs in interneuron-motoneuron pairs. (**A**) Simultaneous whole-cell patch-clamp recording from a spinal interneuron (current clamp, upper traces) and a putative motoneuron (voltage clamp, lower traces). In part a, three individual IPSCs were evoked by single presynaptic action potentials (5-ms, 380-pA pulses). In part b, IPSCs were evoked by a train of presynaptic action potentials (55-ms, 380-pA pulse). The inset shows a schematic representation of the paired recording configuration. In part c, the locations of presynaptic interneuron somata are shown superimposed with a schematic drawing of the cytoarchitechtonic layers of the deep lumbar rat spinal cord. (**B**) Unitary IPSCs in a pair, part a, before antagonist application, part b, in the presence of 400 nM strychnine, and part c, in the presence of 400 nM strychnine plus 5 μM bicuculline. Lower traces in parts b and c are shown at an expanded amplitude scale. The traces represent averages from 3 (part a) or 10 (parts b and c) single sweeps, obtained at the end of the control period and the antagonist washin periods, respectively. (**C**) Peak amplitude of single unitary IPSCs plotted against time during the application of strychnine and bicuculline as indicated by the horizontal bars. Same pair as shown in (B). Inset shows a histogram of the relative contribution of the $GABA_A$R-mediated component to the peak IPSC, estimated from the amplitude of the strychnine-resistant component and the strychnine block of GABA-activated currents (Fig. 4C).

ceptor ($GABA_A$R) subunit, and gephyrin immunoreactivity are present in postsynaptic densities (*4*). This supports the hypothesis of a glycine- and GABA-mediated cotransmission in the mammalian spinal cord (*5*).

We examined the cotransmission hypothesis directly, using dual whole-cell patch-clamp recordings from synaptically coupled pairs of interneurons and putative motoneurons in slices from neonatal rats (Fig. 1) (*6, 7*). Unitary inhibitory postsynaptic currents (IPSCs) evoked in motoneurons by single action potentials in presynaptic interneurons showed a rapid rise (20 to 80% rise time of 0.46 ± 0.05 ms at 22° to 25°C, n = 11; Fig. 1A). The mean peak amplitude (including failures of transmission) was 330 ± 99 pA (−50 mV), corresponding to the opening of ~100 channels (*8*). The short and constant latency (2.85 ± 0.19 ms; Fig. 1A) and the small percentage of failures (16.4 ± 6.7%) indicated that the IPSCs were monosynaptic in origin. Unitary IPSCs evoked by presynaptic action potential trains exhibited marked facilitation of the IPSC amplitude (Fig. 1A). These functional properties of unitary IPSCs were similar to those reported with minimal extracellular stimulation (*9*).

We next determined the contribution of GlyRs and $GABA_A$Rs to the unitary IPSCs in pairs using the antagonists strychnine and bicuculline. The GlyR antagonist strychnine (*10*), added to the bath solution at a concentration of 400 nM (8 pairs) or 1 μM (3 pairs), blocked the unitary IPSC completely in only 2 of 11 interneuron-motoneuron pairs. In 9 of 11 pairs, a strychnine-resistant component remained that decayed more slowly than the strychnine-sensitive component (Fig. 1B) and, on average, contributed 15 ± 5% to the total peak current amplitude (range of 4 to 53%). In 9 of 9 pairs, the strychnine-resistant

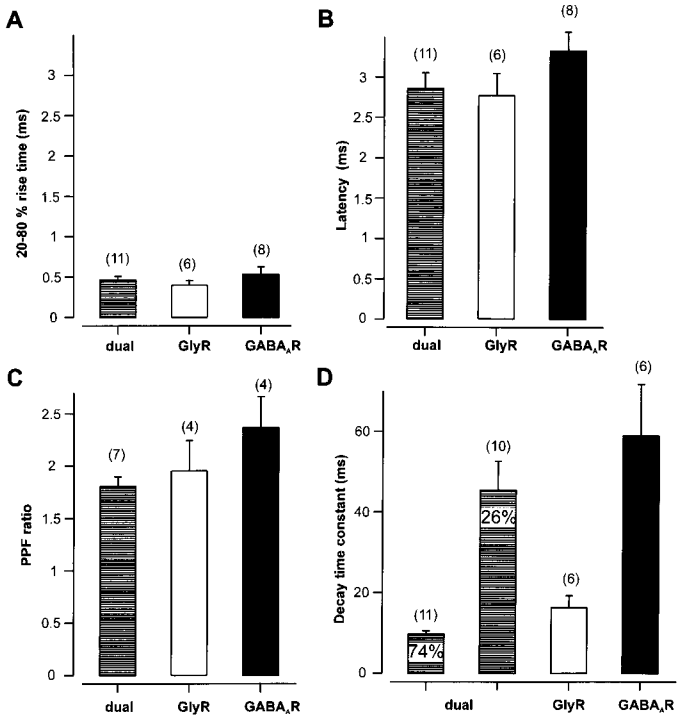

Fig. 2. Comparison of the functional properties of GlyR- and $GABA_A$R-mediated IPSC components. Hatched bars, unitary IPSC in control conditions; open bars, GlyR-mediated component (in the presence of bicuculline in three pairs, and in control conditions in three additional pairs in which subsequent strychnine application blocked >95% of the IPSC); filled bars, $GABA_A$R-mediated component (in the presence of strychnine in the pairs that showed the largest $GABA_A$R-mediated component). (**A**) The 20 to 80% rise time of the IPSC. (**B**) Synaptic latency, measured from the rising phase of the presynaptic action potential to the beginning of individual IPSCs. (**C**) Paired-pulse facilitation ratio (PPF; amplitude of the second IPSC relative to that of the first IPSC, both measured from the baseline preceding the first IPSC, 10-ms interval). (**D**) Decay time constants of the IPSC. For the unitary IPSC in control conditions, τ_1 and τ_2 from the bi-exponential fit are specified separately (amplitude contribution plotted within bar). For the isolated GlyR-mediated and $GABA_A$R-mediated component the mean of τ_1 and τ_2, weighted with the respective amplitude contribution, is given. Number of pairs is indicated in parentheses.

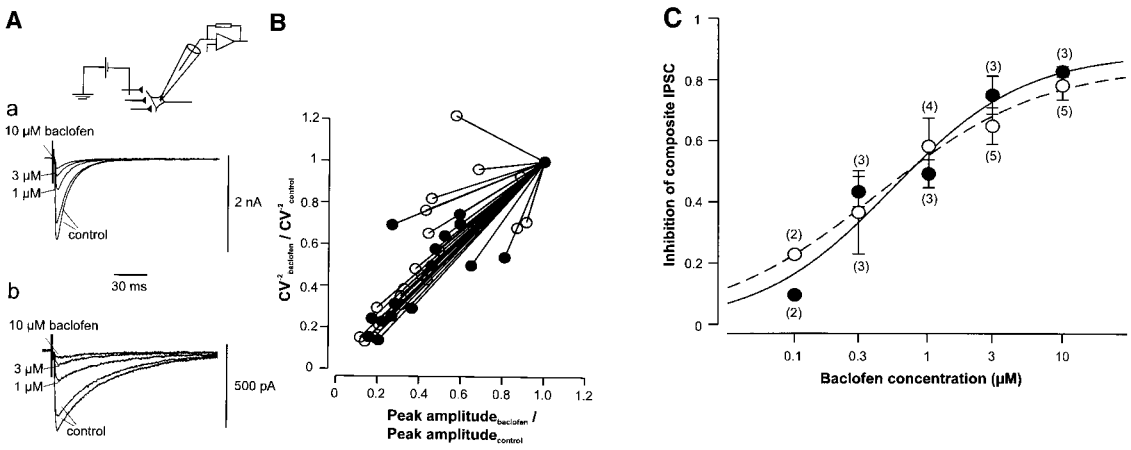

Fig. 3. Comodulation of GlyR- and $GABA_A$R-mediated IPSC components by presynaptic $GABA_B$ receptors. (**A**) Inhibition of composite IPSCs by 1, 3, and 10 μM *R*-(−)-baclofen. Part a shows the GlyR-mediated IPSC in the presence of 5 μM bicuculline, and part b shows the $GABA_A$R-mediated IPSC in the presence of 400 nM strychnine, average of 10 single sweeps each. The bath solution contained 5 μM CNQX and 25 μM D-AP5 in both cases. The inset shows a schematic representation of the method of extracellular stimulation of presynaptic axons and the postsynaptic recording configuration. (**B**) The coefficient of variation to the −2 power (CV^{-2}) of the IPSC peak amplitude in the presence of baclofen was plotted against the mean in the presence of baclofen, both normalized by the respective control values (*12*). The CV and mean were calculated from 40 evoked IPSCs. Data points for both GlyR- (open circles) and $GABA_A$R-mediated (filled circles) component were adjacent to the identity line, confirming the presynaptic nature of the effect. (**C**) Inhibition of the GlyR-mediated component (open circles) and the $GABA_A$R-mediated component (filled circles) of the IPSC by baclofen, plotted against baclofen concentration. Data points were fit with the equation $f = A/[1 + (IC_{50}/c)^n]$, where IC_{50} is the half-maximal inhibitory concentration, *n* the Hill coefficient, *c* the baclofen concentration, and *A* the maximal effect. The IC_{50} values were 0.41 μM (n = 0.70, A = 0.85; GlyR-mediated component, dashed curve) and 0.53 μM (n = 0.88, A = 0.89; $GABA_A$R-mediated component, solid curve), respectively. Number of motoneurons indicated in parentheses.

IPSC component was abolished by the $GABA_A$R antagonist bicuculline (5 μM; Fig. 1, B and C). Thus, unitary IPSCs at spinal inhibitory synapses comprised GlyR- and $GABA_A$R-mediated components that could be dissected pharmacologically.

A comparison of the functional properties of the GlyR- and the $GABA_A$R-mediated component of the evoked unitary IPSC indicated that the two components were not significantly different in the 20 to 80% rise time (0.40 ± 0.06 ms versus 0.53 ± 0.09 ms; Fig. 2A; $P > 0.1$), the synaptic latency (2.8 ± 0.3 ms versus 3.3 ± 0.2 ms; Fig. 2B; $P > 0.1$), or the paired-pulse facilitation ratio (1.95 ± 0.29 versus 2.36 ± 0.30; Fig. 2C; $P > 0.1$). However, they differed markedly in the decay time course; the decay

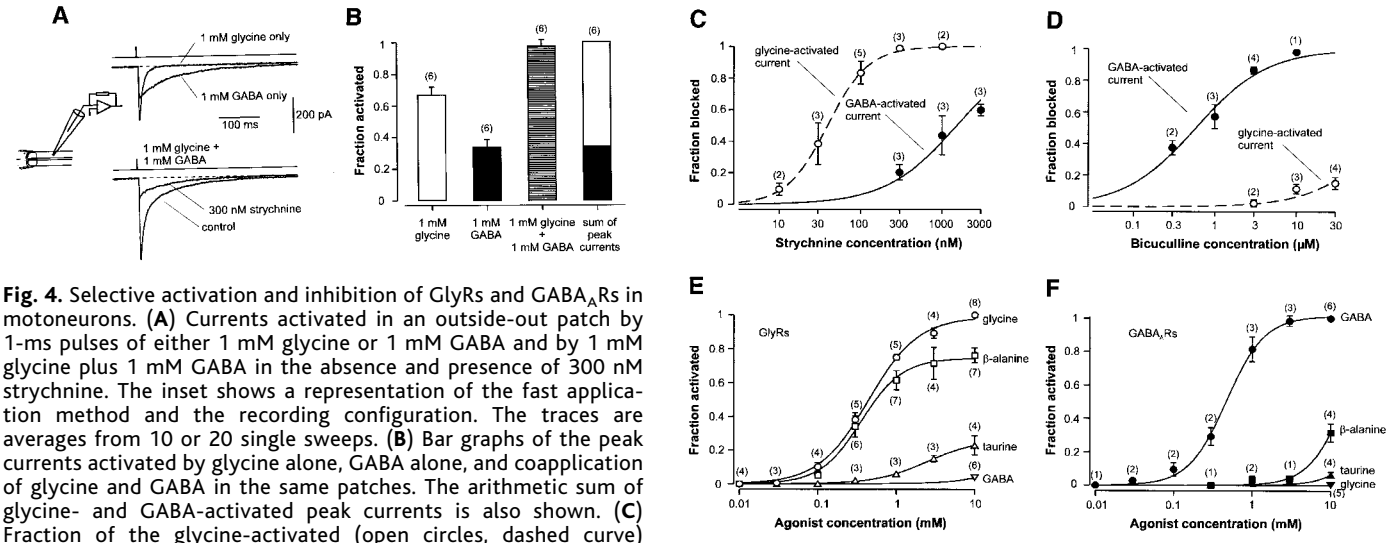

Fig. 4. Selective activation and inhibition of GlyRs and $GABA_A$Rs in motoneurons. (**A**) Currents activated in an outside-out patch by 1-ms pulses of either 1 mM glycine or 1 mM GABA and by 1 mM glycine plus 1 mM GABA in the absence and presence of 300 nM strychnine. The inset shows a representation of the fast application method and the recording configuration. The traces are averages from 10 or 20 single sweeps. (**B**) Bar graphs of the peak currents activated by glycine alone, GABA alone, and coapplication of glycine and GABA in the same patches. The arithmetic sum of glycine- and GABA-activated peak currents is also shown. (**C**) Fraction of the glycine-activated (open circles, dashed curve) and the GABA-activated current (filled circles, solid curve) blocked by strychnine added to control barrel solution, plotted against strychnine concentration. Data points were fit with the equation given in the legend to Fig. 3. The IC_{50} values were 39 nM (n = 1.73, A constrained to 1) and 1.5 μM (*n* and *A* constrained to 1), respectively. (**D**) Fraction of GABA-activated (filled circles, solid curve) and glycine-activated current (open circles, dashed curve) blocked by bicuculline added to control barrel solution, plotted against bicuculline concentration. The IC_{50} values were 0.58 μM (n = 0.99, A constrained to 1) and 144 μM (*n* and *A* constrained to 1), respectively. (**E**) GlyR activation by glycine, β-alanine, taurine, and GABA. The peak amplitudes of the agonist-activated currents were normalized to the peak current activated by 10 mM glycine in the same patches and were plotted against agonist concentration. $GABA_A$Rs were blocked by 10 μM bicuculline (both barrels). Estimated EC_{50} values were 441 μM (n = 1.4, A = 0.99), 359 μM (n = 1.7, A = 0.74), 2.46 mM (n = 1.3, A = 0.26), and 105 mM (*n* constrained to 1.4, *A* constrained to 1). (**F**) $GABA_A$R activation by GABA, β-alanine, taurine, and glycine. The peak amplitudes of the agonist-activated currents were normalized to the peak current activated by 10 mM GABA in the same patches and were plotted against agonist concentration. GlyRs were blocked by 1 μM strychnine (both barrels). Estimated EC_{50} values were 472 μM (n = 1.8, A = 1.02), 15.1 mM (n = 1.9, A constrained to 1), 44.2 mM (*n* constrained to 1.8, *A* constrained to 1), and 236 mM (*n* constrained to 1.8, *A* constrained to 1). Duration of agonist pulses was 1 ms in all experiments. Number of patches (sometimes with multiple measurements) is indicated in parentheses.

time constant of the GlyR-mediated component was, on average, a factor of 3.6 faster than that of the $GABA_A$R-mediated component (16.3 ± 3.0 ms versus 58.9 ± 12.8 ms; Fig. 2D; $P < 0.01$).

To examine a possible differential modulation of GlyR- and $GABA_A$R-mediated components by presynaptic $GABA_B$ receptors, we investigated the effects of the $GABA_B$ receptor agonist *R*-(−)-baclofen on composite IPSCs evoked by extracellular stimulation of presynaptic axons (Fig. 3) (*6, 11*). Baclofen reduced the peak amplitude of both the GlyR-mediated component (in the presence of bicuculline) and the $GABA_A$R-mediated component (in the presence of strychnine) (Fig. 3A). Plots of the coefficient of variation to the −2 power against the mean value of the IPSC, both normalized to the respective control values (*12*), revealed that the data points were located close to the identity line, indicating that the inhibition was presynaptic in origin (Fig. 3B). The concentration dependence of the baclofen effects was almost indistinguishable for the GlyR- and the $GABA_A$R-mediated component (Fig. 3C). Similarly, the metabotropic glutamate receptor agonist L-AP4 (25 μM) reduced the peak amplitude of both components to the same extent (to 55.4 ± 13.7% and 46.2 ± 5.8% of the control value, respectively, four motoneurons in each case). These results suggest comodulation of GlyR- and $GABA_A$R-mediated components of the IPSC by the same set of presynaptic receptors.

Although these findings appeared to be consistent with a corelease of glycine and GABA at inhibitory synapses in the spinal cord, this conclusion relies on the assumptions that glycine and GABA activate separate receptors, and that strychnine and bicuculline block these receptors selectively. We thus applied brief (1-ms) pulses of the putative transmitters to outside-out patches isolated from motoneuron somata (Fig. 4) (*6, 13*). Both glycine and GABA evoked detectable currents in the majority of patches (19 of 23 patches); the peak amplitude of the current evoked by 1 mM glycine in these patches was on average a factor of 2.5 larger than that activated by 1 mM GABA (Fig. 4A). The current activated by coapplication of 1 mM glycine and 1 mM GABA was 97.5 ± 3.9% of the arithmetic sum of the glycine- and GABA-activated currents in the same patches (six patches), indicating that glycine and GABA activated molecularly distinct receptors (Fig. 4B).

The antagonist strychnine blocked the glycine-activated current with an IC_{50} of 39 nM (Fig. 4, A and C), whereas the GABA-activated current was affected only at several-fold higher concentrations (IC_{50} = 1.5 μM). Conversely, bicuculline blocked the GABA-activated current with an IC_{50} of 0.58 μM (Fig. 4D), whereas the glycine-activated current was almost unaffected by concentrations up to 30 μM (estimated IC_{50} = 144 μM). Thus, strychnine and bicuculline blocked spinal GlyRs and $GABA_A$Rs with high (but not absolute) selectivity.

Although synaptic corelease of glycine and GABA is the most likely interpretation of the above results, an alternative possibility would be that a third transmitter, such as β-alanine or taurine, coactivated postsynaptic GlyRs and $GABA_A$Rs (*14*). We therefore compared the affinity of both types of receptors for glycine and GABA with that for β-alanine and taurine. Glycine and GABA activated GlyRs and $GABA_A$Rs at low concentrations; the half-maximal activating concentrations (EC_{50}'s) were 441 μM and 472 μM, respectively, with 1-ms agonist pulses (Fig. 4, E and F). In contrast, GABA at concentrations as high as 10 mM was unable to activate GlyRs (Fig. 4E), and conversely, glycine was unable to activate $GABA_A$Rs (Fig. 4F). β-Alanine appeared to be a partial agonist for GlyRs (Fig. 4E), but it hardly activated $GABA_A$Rs (Fig. 4F). Finally, taurine showed very low affinity for both types of receptors (Fig. 4, E and F). These results further support the hypothesis that glycine and GABA are coreleased at inhibitory spinal synapses (*15*).

We next examined GlyR- and $GABA_A$R-mediated components in spontaneous miniature IPSCs (Fig. 5) (*6, 16*), presumably generated by the release of the contents of single synaptic vesicles (*17*). To enhance the difference in decay time course between the two components, we added the benzodiazepine flunitrazepam (*18*). Flunitrazepam (2 μM) slowed selectively the decay of the $GABA_A$R-mediated component of the evoked compound IPSC; the decay of the $GABA_A$R-mediated component was, on average, prolonged by a factor of 1.65 ± 0.18 (six motoneurons), whereas that of the GlyR-mediated component was almost unchanged (factor of 0.95 ± 0.05 change, four cells). In the presence of 2 μM flunitrazepam, subsets of individual miniature IPSCs and the average miniature IPSC showed a

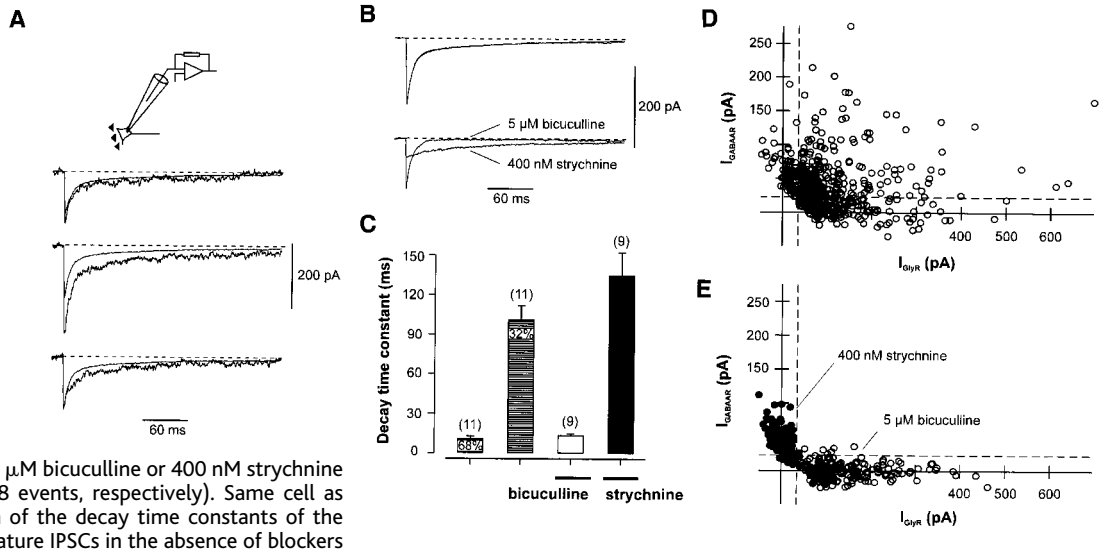

Fig. 5. GlyR- and $GABA_A$R-mediated components in spontaneous miniature IPSCs distinguishable in the presence of flunitrazepam. (**A**) Three examples of spontaneous miniature IPSCs in control conditions recorded from a putative motoneuron in the whole-cell configuration in the presence of 500 nM tetrodotoxin and 2 μM flunitrazepam, superimposed with the average from 49 events. The inset shows a representation of the recording configuration. (**B**) Average miniature IPSCs recorded in the absence (upper trace) and presence of either 5 μM bicuculline or 400 nM strychnine (lower traces, from 17 and 18 events, respectively). Same cell as shown in (A). (**C**) Comparison of the decay time constants of the dual-component average miniature IPSCs in the absence of blockers (hatched bars, respective amplitude contributions plotted within bars) with those recorded in the presence of 5 μM bicuculline (open bars) or 400 nM strychnine (filled bars). Number of motoneurons is indicated in parentheses. (**D** and **E**) Scatter plots of the amplitude of the $GABA_A$R-mediated component (I_{GABAAR}) against that of the GlyR-mediated component (I_{GlyR}) in miniature IPSCs obtained by template fit analysis in the absence of blockers [(D), 560 events] and in the presence of 5 μM bicuculline [(E), open circles, 200 events] or 400 nM strychnine [(E), filled circles, 125 events]. Dashed lines indicate the +2σ ranges of the data points in the presence of antagonists. Positive amplitude values indicate inward currents. Occasional negative amplitude values arose from noise superimposed on miniature events. Data pooled from five motoneurons.

bi-exponential decay (Fig. 5A). In the presence of 5 μM bicuculline, the decay time course of the miniature IPSCs was fast, similar to that of the first component in control conditions, whereas in the presence of 400 nM strychnine, the decay was slow, comparable to that of the second component in the absence of antagonists (Fig. 5, B and C).

To quantify the amplitude contributions of the two components in individual miniature IPSCs, we obtained average GlyR- and $GABA_A$R-mediated miniature IPSC templates in the presence of either bicuculline or strychnine. Subsequently, individual miniature events recorded from the same neuron before antagonist application were fit with the sum of these two templates, multiplied by variable amplitude factors (*16*). Scatter plots of the amplitudes of the two components indicated that in control conditions a large proportion of data points fell into the first quadrant (Fig. 5D), indicating a high percentage of dual-component events. In contrast, data points in the presence of antagonists were clustered around the axes (Fig. 5E), showing that dual-component events were largely absent. Defining the criterion separating the dual- and monocomponent events at the $\pm 2\sigma$ ranges of the data points in the presence of either bicuculline or strychnine, we classified 44% of miniature IPSCs in control conditions as dual-component, 41% as pure GlyR-mediated, and 15% as pure $GABA_A$R-mediated events. If miniature IPSCs reflect the fusion of individual synaptic vesicles (*17*), these results would indicate both the costorage of glycine and GABA in the same synaptic vesicle and the colocalization of GlyRs and $GABA_A$Rs in the same postsynaptic density.

In conclusion, we showed that unitary IPSCs and subsets of miniature IPSCs at inhibitory synapses in the spinal cord are dual-component events comprising GlyR- and $GABA_A$R-mediated components. On the basis of the strychnine sensitivity (Fig. 4C) and the different decay time constants of GlyR- and $GABA_A$R-mediated currents, we estimate that the GlyR-mediated component dominates the IPSC peak amplitude (81%), whereas the $GABA_A$R-mediated component dominates the inhibitory postsynaptic charge (68%).

The most likely explanation for the dual-component nature of the unitary IPSC is the quantal corelease of glycine and GABA from a single spinal interneuron. None of the plausible transmitter candidates coactivates both types of receptors. The dual-component nature of a subset of miniature IPSCs suggests the strictest possible form of corelease, that is, from the same synaptic vesicle. This is compatible with the observation that vesicular transporters at inhibitory synapses accept both glycine and GABA as substrates (*19*). Whether glycine- and GABA-mediated cotransmission is a general principle of inhibition that also applies to subcortical neuronal circuitries (for example, the auditory pathway) (*20*) remains to be addressed.

Glycine- and GABA-mediated cotransmission could support the precise regulation of the time course of the postsynaptic conductance by the relative amount of glycine and GABA released from the presynaptic interneuron. This could be of critical importance for motor coordination (*21*) and the generation of locomotor patterns (*22*). Cotransmission would also enable feedback control of transmitter release by presynaptic $GABA_B$ receptors, which may not be possible at pure glycinergic synapses. Finally, cotransmission may enable compensatory mechanisms in genetic GlyR subunit defects (*23*).

References and Notes

1. R. A. Nicoll, *Science* **241**, 545 (1988).
2. T. Hökfelt, *Neuron* **7**, 867 (1991).
3. D. R. Curtis, L. Hösli, G. A. R. Johnston, *Exp. Brain Res.* **6**, 1 (1968); S. Cullheim and J.-O. Kellerth, *J. Physiol. London* **312**, 209 (1981); S. P. Schneider and R. E. W. Fyffe, *J. Neurophysiol.* **68**, 397 (1992).
4. A. J. Todd and A. C. Sullivan, *J. Comp. Neurol.* **296**, 496 (1990); G. Örnung *et al.*, *ibid.* **365**, 413 (1996); A. J. Todd, C. Watt, R. C. Spike, W. Sieghart, *J. Neurosci.* **16**, 974 (1996); S. Bohlhalter, H. Mohler, J.-M. Fritschy, *Brain Res.* **642**, 59 (1994).
5. A. Triller, F. Cluzeaud, H. Korn, *J. Cell. Biol.* **104**, 947 (1987); see also G. Burnstock, *Neuroscience* **1**, 239 (1976).
6. Transverse slices (400 to 500 μm thickness) were cut from the deep lumbar region of the spinal cord of 5- to 10-day-old (mainly 6- or 7-day-old) Wistar rats with a vibratome (DTK-1000, Dosaka). Animals were killed by decapitation, in accordance with institutional guidelines. Motoneurons were tentatively identified by their location in the ventral horn and the large diameter of the soma (>20 μm) with infrared differential interference contrast videomicroscopy [G. J. Stuart, H.-U. Dodt, B. Sakmann, *Pfluegers Arch.* **423**, 511 (1993)]; mainly motoneurons in the medial pool were investigated. For the synaptic experiments, the physiological extracellular solution contained 125 mM NaCl, 25 mM $NaHCO_3$, 25 mM glucose, 2.5 mM KCl, 1.25 mM NaH_2PO_4, 2 mM $CaCl_2$, and 1 mM $MgCl_2$. Slices were continuously superfused with this solution; the flow rate was increased to ~12 ml min^{-1} during solution exchange (chamber volume of 2 ml). The internal solution contained 140 or 145 mM KCl, either 0.1 mM (pre- or postsynaptic neuron) or 10 mM EGTA (only postsynaptic neuron), and 2 mM $MgCl_2$, 2 mM adenosine 5′-triphosphate disodium salt, and 10 mM Hepes (pH adjusted to 7.3 with KOH). In some experiments 10 or 20 mM sucrose was added to stabilize the series resistance of the recordings. For the fast application experiments, the Na^+-rich external solution contained 135 mM NaCl, 5.4 mM KCl, 1.8 mM $CaCl_2$, 1 mM $MgCl_2$, and 5 mM Hepes (pH adjusted to 7.2 with NaOH), and the internal solution for filling the patch pipette was a K^+-rich solution containing 10 mM EGTA. Strychnine hydrochloride (S-8753, 44H0910), (−)-bicuculline methiodide (B-6889, 36H3897), and flunitrazepam were from Sigma, *R*-(−)-baclofen from Novartis (charge 3), 6-cyano-7-nitroquinoxaline-2,3-dione (CNQX), D-2-amino-5-phosphonopentanoic acid (D-AP5), and L-2-amino-4-phosphonobutyric acid (L-AP4) from Tocris, and tetrodotoxin (TTX) from Molecular Probes. Stock solutions were made in distilled water, NaOH (for CNQX and L-AP4), or dimethyl sulfoxide (for flunitrazepam and baclofen, concentration of dimethyl sulfoxide in the final solution ≤0.1%). The holding potential of the whole-cell recorded putative motoneuron was set to −50 mV. In the patch experiments, the holding potential was 0 mV and the membrane potential was stepped to −50 mV before the concentration jump. The recording temperature was 22° to 25°C. IPSCs and glycine- or GABA-activated currents were filtered at 5 kHz (4-pole low-pass Bessel) and digitized at 10 or 20 kHz with a 1401plus interface (Cambridge Electronic Design). IPSC traces shown in the figures were filtered digitally at 1 or 2 kHz (Gaussian characteristics). The decay was fit with the sum of two exponentials; the time constants are given either separately or as an amplitude-weighted mean. All values are given as mean ± SEM; error bars in the figures also represent SEM. Statistical significance was assessed by Student's *t* test at the significance level (*P*) indicated.
7. To evoke unitary IPSCs, we made simultaneous whole-cell patch-clamp recordings [R. Miles and R. K. S. Wong, *J. Physiol.* (*London*) **356**, 97 (1984); J. R. P. Geiger, J. Lübke, A. Roth, M. Frotscher, P. Jonas, *Neuron* **18**, 1009 (1997)] from synaptically connected interneurons and putative motoneurons using two independent Axopatch 200A amplifiers (Axon Instruments). Interneurons presynaptic to a whole-cell recorded motoneuron were identified by pressure application of the non-desensitizing glutamate receptor agonist kainate (150 μM) [E. Jankowska and W. J. Roberts, *J. Physiol.* (*London*) **222**, 623 (1972)] with a Picospritzer II (General Valve, pressure ~0.7 bar, pulse duration ~5 ms, pipette tip diameter ~1 μm); they had characteristically small somata (mean transverse diameter 12 μm). Patch pipettes were pulled from borosilicate glass tubing (2 mm outer diameter and 0.4 or 0.5 mm wall thickness); the resistance was 0.6 to 1.5 Mohm for the postsynaptic and 1.5 to 5 Mohm for the presynaptic neurons. Recordings from the postsynaptic neuron were made in the voltage-clamp configuration with series resistance (R_S) compensation (nominally 80 to 90%, lag 20 to 100 μs; R_S before compensation 2 to 15 Mohm). The presynaptic interneuron was held in the current-clamp configuration at −70 mV, and depolarizing current pulses were applied at a frequency of 0.25 to 1 s^{-1}.
8. J. Bormann, O. P. Hamill, B. Sakmann, *J. Physiol.* (*London*) **385**, 243 (1987); T. Takahashi and A. Momiyama, *Neuron* **7**, 965 (1991).
9. T. Takahashi, *J. Physiol.* (*London*) **450**, 593 (1992).
10. C.-M. Becker, in *Handbook of Experimental Pharmacology*, H. Herken and F. Hucho, Eds. (Springer-Verlag, Berlin, 1992), pp. 539–575.
11. Composite IPSCs were evoked by extracellular stimulation of axons close to the whole-cell recorded putative motoneuron in the presence of 5 μM CNQX and 25 μM D-AP5. Electrical stimuli (5 to 50 V, 200 μs) were applied through a glass pipette with a tip diameter of 2 to 3 μm, filled with Na^+-rich external solution.
12. R. Malinow and R. W. Tsien, *Nature* **346**, 177 (1990).
13. Glycine, GABA, β-alanine, and taurine were applied rapidly [D. Colquhoun, P. Jonas, B. Sakmann, *J. Physiol.* (*London*) **458**, 261 (1992)] to outside-out patches isolated from the somata of putative motoneurons. The resistance of the patch pipettes used in these experiments was 1.5 to 5 Moms. The 20 to 80% solution exchange time, measured from the open tip response, was 70 to 200 μs.
14. B. Laube, D. Langosch, H. Betz, V. Schmieden, *Neuroreport* **6**, 897 (1995); V. Schmieden, J. Kuhse, H. Betz, *Science* **262**, 256 (1993); M. V. Jones and G. L. Westbrook, *Neuron* **15**, 181 (1995); W. J. Zhu and S. Vicini, *J. Neurosci.* **17**, 4022 (1997).
15. Synaptic release of β-alanine was further unlikely, because the decay of the β-alanine–activated currents was much faster than that of the IPSC components. When GlyRs or $GABA_A$Rs were activated by 1-ms pulses of 10 mM β-alanine, the respective currents decayed with time constants of 6.4 ± 0.3 ms (n = 8) and 3.8 ± 0.9 ms (n = 4), respectively. In contrast, the mean glycine (10 mM)–activated current decayed with a time constant of 20.3 ± 1.6 ms (n = 24), and the GABA (10 mM)–activated current with a time constant of 50.0 ± 4.3 ms (n = 16), similar to the IPSC components.
16. Miniature IPSCs were recorded in the presence of 500 nM TTX, 5 μM CNQX, and 25 μM D-AP5 (conditions otherwise identical to those in the paired recording experiments). Events were detect-

ed with an algorithm based on an optimally scaled template [P. Jonas, G. Major, B. Sakmann, *J. Physiol.* (*London*) **472**, 615 (1993)]; the threshold values were 0.8 ms for the 20 to 80% rise time and 25 to 50 pA for the peak amplitude. In the miniature IPSC experiments analyzed, the average frequency in control conditions was less than 2 Hz; superposition of independent miniature IPSCs by chance was thus unlikely. To quantify the contribution of GlyR- and $GABA_A$R-mediated components in miniature IPSCs, we fit individual events with the function $f(t) = A_0 + A_1 I_{GlyR}(t) + A_2 I_{GABAAR}(t)$, where $I_{GlyR}(t)$ and $I_{GABAAR}(t)$ were average miniature IPSC templates obtained in the presence of bicuculline and strychnine, respectively (baseline subtracted, peak amplitude normalized to 1). Variables A_1 and A_2 were obtained by multiple linear regression.

17. B. Katz, *The Release of Neural Transmitter Substances* (Liverpool Univ. Press, Liverpool, 1969); J. M. Bekkers and C. F. Stevens, *Nature* **341**, 230 (1989).
18. J. R. Mellor and A. D. Randall, *J. Physiol.* (*London*) **503**, 353 (1997).
19. P. M. Burger *et al.*, *Neuron* **7**, 287 (1991); C. Sagné *et al.*, *FEBS Lett.* **417**, 177 (1997).
20. J. M. Juiz, R. H. Helfert, J. M. Bonneau, R. J. Wenthold, R. A. Altschuler, *J. Comp. Neurol.* **373**, 11 (1996).
21. J. C. Eccles, *The Physiology of Synapses* (Springer-Verlag, Berlin, 1964).
22. J. Tegnér, T. Matsushima, A. El Manira, S. Grillner, *J. Neurophysiol.* **69**, 647 (1993).
23. W. Brune *et al.*, *Am. J. Hum. Genet.* **58**, 989 (1996).
24. We thank J. R. P. Geiger, M. V. Jones, M. Martina, and K. Starke for critically reading the manuscript, and B. Sakmann for helpful discussions. We also thank B. Hillers for secretarial assistance, S. Pfitzinger for construction of equipment, and Novartis for providing baclofen. Supported by the DFG (grant Jo-248/2-1 and Sa-435/10-2).

30 March 1998; accepted 9 June 1998

Spatial Organization of Transcription Elongation Complex in *Escherichia coli*

Evgeny Nudler,* Ivan Gusarov, Ekaterina Avetissova, Maxim Kozlov, Alex Goldfarb

During RNA synthesis in the ternary elongation complex, RNA polymerase enzyme holds nucleic acids in three contiguous sites: the double-stranded DNA-binding site (DBS) ahead of the transcription bubble, the RNA-DNA heteroduplex-binding site (HBS), and the RNA-binding site (RBS) upstream of HBS. Photochemical cross-linking allowed mapping of the DNA and RNA contacts to specific positions on the amino acid sequence. Unexpectedly, the same protein regions were found to participate in both DBS and RBS. Thus, DNA entry and RNA exit occur close together in the RNA polymerase molecule, suggesting that the three sites constitute a single unit. The results explain how RNA in the integrated unit RBS–HBS–DBS may stabilize the ternary complex, whereas a hairpin in RNA result in its dissociation.

The paradox of transcription elongation is the ability of RNA and DNA to pass through RNA polymerase (RNAP) within an extremely stable ternary complex. To explain protein–DNA–RNA interaction that is both tight and flexible, investigators have proposed the concept of the sliding clamp (*1, 2*) by analogy with the DNA replication apparatus (*3*).

In our current thinking, the sliding clamp consists of three putative elements (Fig. 1). DBS, which is defined as the region of strong nonionic interaction between RNAP and the template, has been mapped to ~9 base pairs (bp) of DNA duplex just ahead of the point where DNA forks out into the transcription bubble (*2*). Recently, we presented evidence that the template DNA strand in the bubble forms an ~8-bp hybrid (*4*), which is held in RNAP by weak ionic interactions (*2*) that define HBS. The notion of a distinct site holding single-stranded RNA leading out of the active center (RBS), first proposed two decades ago (*5*), has been extensively discussed recently (*6*). Together, HBS and RBS should cover 14 to 16 3′-proximal nucleotides of RNA, in accord with ribonuclease protection data (*5, 7, 8*). The observation that the RNA secondary structure (hairpins) at 7 to 9 nucleotides from the 3′ terminus destabilizes the ternary elongation complex (TEC) (*9*) indicates that this may be the area of crucial protein-RNA interactions. Here we directly identify RNA, DNA, and protein segments involved in close contacts. The results show that RBS, HBS, and DBS are integrated in the RNAP molecule, which has important implications for the mechanism of RNA chain elongation and termination.

To map RNA-protein contacts along the trajectory of RNA, we used a photoreactive analog of uridine, 4-thio-uridine (Fig. 2A), incorporated into a single position of RNA transcript. The probe has a reagent arm less than 1 Å long and passes unimpeded through the protein as the complex advances (Fig. 2B). We induced cross-linking by ultraviolet (UV) irradiation of TEC that has been stalled at defined positions. The probe was incorporated at either position +21 or +45 relative to the RNA 5′ terminus (Fig. 2B, lanes 2 to 14 and 15 to 18, respectively).

Judging from the relative yield of cross-linking with the +21 probe, close RNA contacts with RNAP β′ subunit, and to a lesser extent with the β subunit, occur near the active site (position −1 relative to the 3′ terminus). The segment of at least four nucleotides from −3 to −6 appears not to be involved in close β′,β contacts. Further upstream, the close contacts (β′ ≫ β) occur within the nine-nucleotide segment from −10 to −18. Because of the sequence constraints, contacts at −7 to −9 could not be scanned with the +21 probe. However, with the +45 probe (lanes 15 to 18), RNA nucleotide at −8 displays a cross-linking yield of intermediate intensity, suggesting that it is on the borderline of the close RNA-protein contact area. In the case of the +45 probe, two β′–cross-linked species could be resolved (lanes 17 and 18) because of the longer RNA moiety.

Qualitatively similar results were obtained when the azido-uridine probe with longer (~8 Å) reagent arm was used (Fig. 2A), but the difference between cross-linking of different transcript segments was less pronounced (*8*).

For unambiguous interpretation of the results, it was essential to establish that the stalled TECs used for cross-linking were not backtracked (*4, 7*) (Fig. 2C). To this end, a control experiment was performed in which backtracking in TEC56 (cross-linking probe at −12) was either induced or suppressed by incorporating helix-destabilizing (inosin) or stabilizing [5-bromo-uridine triphosphate (5-bromo-UTP) and 5-iodo-cytosine triphosphate (5-iodo-CTP)] nucleotides, respectively, into the 3′ proximal region of the transcript (*4*). The backtracked complex was identified by its failure to elongate RNA (Fig. 2C, bottom panel, lane 4) and by its sensitivity to transcript cleavage factor GreB (lane 5). Evidently, prominent RNA-protein cross-linking occurred only in the productive complex, not in the backtracked complex (Fig. 2C, top panel). In addition, antisense oligonucleotides known to inhibit backtracking (*7*) had no effect on the cross-linking results obtained with TEC30, TEC34, and TEC38 (*8*).

To map the cross-linking sites, we excised from the gel of Fig. 2B the species of β or β′ cross-linked to RNA. The analysis was performed for TECs with the probe positioned at +21 (TEC30, TEC34, TEC38, TEC43, and

E. Nudler and I. Gusarov, Department of Biochemistry, New York University Medical Center, New York, NY 10016, USA. E. Avetissova, M. Kozlov, A. Goldfarb, Public Health Research Institute, New York, NY 10016, USA.

*To whom correspondence should be addressed. E-mail: evgeny.nudler@med.nyu.edu